AGU PUBLICATIONS

Earth and Space Science

RESEARCH ARTICLE
10.1002/2016EA000228

Key Points:
- We revisit a statistical methodology that helps the analysis for satellite remote sensing of trace gases like carbon dioxide
- We analyze the errors that appear due to the difference of the a priori climatology and the true state
- This methodology may help capture the intrinsic discrepancy and relation in various retrieval scenarios

Correspondence to:
Z. Su,
zssu@caltech.edu

Citation:
Su, Z., Y. L. Yung, R.-L. Shia, and C. E. Miller (2017), Assessing accuracy and precision for space-based measurements of carbon dioxide: An associated statistical methodology revisited, *Earth and Space Science*, *4*, 147–161, doi:10.1002/2016EA000228.

Received 10 OCT 2016
Accepted 16 FEB 2017
Accepted article online 24 FEB 2017
Published online 29 MAR 2017

Assessing accuracy and precision for space-based measurements of carbon dioxide: An associated statistical methodology revisited

Zhan Su[1], Yuk L. Yung[1], Run-Lie Shia[1], and Charles E. Miller[2]

[1]Division of Geological and Planetary Sciences, California Institute of Technology, Pasadena, California, USA, [2]Jet Propulsion Laboratory, California Institute of Technology, Pasadena, California, USA

Abstract Analyzing retrieval accuracy and precision is an important element of space-based CO_2 retrievals. However, this error analysis is sometimes challenging to perform rigorously because of the subtlety of *Multivariate Statistics*. To help address this issue, we revisit some fundamentals of Multivariate Statistics that help reveal the statistical essence of the associated error analysis. We show that the related statistical methodology is useful for revealing the intrinsic discrepancy and relation between the retrieval error for a nonzero-variate CO_2 state and that for a zero-variate one. Our study suggests that the two scenarios essentially yield the same-magnitude accuracy, while the latter scenario yields a better precision than the former. We also use this methodology to obtain a rigorous framework systematically and explore a broadly used *approximate* framework for analyzing CO_2 retrieval errors. The approximate framework introduces errors due to an essential, but often forgotten, fact that a priori climatology in reality is never equal to the true state. Due to the nature of the problem considered, realistic numerical simulations that produce synthetic spectra may be more appropriate than remote sensing data for our specific exploration. As highlighted in our retrieval simulations, utilizing the approximate framework may not be universally satisfactory in assessing the accuracy and precision of Xco_2 retrievals (with errors up to 0.17–0.28 ppm and 1.4–1.7 ppm, respectively, at SNR = 400). In situ measurements of CO_2 are needed to further our understanding of this issue and related implications.

1. Introduction

Optimal estimation theory (OET) [*Rodgers*, 1976, 2000] has been extensively applied for the remote sensing or ground-based retrieval of atmospheric quantities such as greenhouse gas (GHG) [*Saitoh et al*., 2009; *Buchwitz et al*., 2012; *Yoshida et al*., 2011]. This method combines measurements and a priori information to obtain a stable optimal retrieval using a Bayesian approach. The error analysis of OET is a crucial component for the remote sensing retrieval of CO_2. Associated with this, this note is motivated by the following three considerations.

1. In applying the OET for retrieving the atmospheric CO_2, it is often difficult to achieve a coherent and systematic error analysis for retrievals (e.g., this may contribute to the problem proposed in point 2 below). This is partially because the related analysis is based on sophisticated Multivariate Statistics [e.g., *Anderson*, 2003]. However, as far as we know, an explicit and careful illustration of the associated fundamentals of Multivariate Statistics has rarely been included in the literature of the remote sensing of CO_2. Many OET practitioners just use some conclusions derived from *Multivariate Statistics* without knowing the conditions that these conclusions are based on, which may often cause problems. Thus, the associated statistical methodology is worthy of revisiting, which is one of the main motivations of this study. In this note we elucidate the statistical fundamentals that can be essential for the understanding of the mathematical nature of the related error analysis. However, we are motivated by more than a pedagogical goal. Our results can be practical and useful tools in performing the error analysis for retrieval of CO_2, as shown in this manuscript.
2. For remote sensing retrievals via OET, it is known that the deviation of a priori climatology from the true state causes complications for the error analysis. Regarding this effect, the retrievals of H_2O, CO, O_3, and CH_4 using TES observations provide valuable references [e.g., *Kulawik et al*., 2006; *Worden et al*., 2004] (see also the Appendix A). However, we note that numerous, but not all [e.g., *Rodgers and Connor*, 2003; *Connor et al*., 2008; *Cressie et al*., 2016], error analyses for the retrieval of CO_2 do not explicitly

emphasize or discuss this effect by applying an approximate framework (detailed in sections 2 and 3). In this note, we explore this issue utilizing fundamental Multivariate Statistics and numerical experiments, although note that our exploration is not exhaustive due to the complication of the problem considered. Our primary results suggest that using the approximate framework may not deliver universally satisfactory performance compared to the rigorous framework. However, due to the nature of the problem considered, we demonstrate that the rigorous framework itself requires complete knowledge of the to-be-retrieved true state. This by definition is impossible to achieve in real-world remote sensing although possible to do in numerical simulations, as in this study, or with in situ measurements. Consequently, we argue that the widely used approximate framework is a useful approximation in real-world remote sensing (detailed at the end of section 2). This, however, does not change the fact that the approximate framework may cause nonnegligible errors in the error analysis. Further, these nonnegligible errors may not be straightforward to evaluate in reality. To our knowledge, the above message is often not well understood by many OET practitioners and is hence worthy a note.

3. The soundings for a nonzero-variate CO_2 state and for a zero-variate CO_2 state (snapshot state) are two important scenarios for satellite measurement [e.g., *Buchwitz et al*., 2012; *Wunch et al*., 2011]. In this note we explore the intrinsic difference and connection between these two scenarios in the error analysis of CO_2 retrievals based on statistical methodology mentioned in point 1. This approach is new and provides insights on applications in other types of error analysis.

To elucidate the three points above, it is useful to briefly introduce the essence of OET, following *Rodgers* [2000] and his notations except otherwise mentioned. The measurement vector $\boldsymbol{y}$ can be described by a physically based forward model $\boldsymbol{F}(\boldsymbol{x})$:

$$\boldsymbol{y} = \boldsymbol{f}(\boldsymbol{x}) + \boldsymbol{\varepsilon}. \tag{1}$$

The forward model $\boldsymbol{F}(\boldsymbol{x})$ in equation (1) typically consists of three major modules: a radiative transfer code, a solar model, and an instrument model [e.g., *Bösch et al*., 2006]. The uncertainties in the forward model parameters (nonretrieved and retrieved) can contribute to the error of retrieval: e.g., due to uncertainties in aerosol optical depth, surface pressure, instrument parameters, spectroscopic, and calibration parameters [*Li et al*., 2016; *Bösch et al*., 2006]. Their associated effects can be represented/parameterized in $\boldsymbol{\varepsilon}$ [e.g., *Reuter et al*., 2010, Table 1; *O'Dell et al*., 2012, equation (2); *Bowman et al*., 2002, 2006]. How to accurately perform this representation/parameterization is a serious issue and is often challenging [e.g., *Kuang et al*., 2002, *O'Dell et al*., 2012]. For example, *Kuang et al.* [2002] and *Bowman et al*. [2006] assume a perfect forward model for their specific research purpose. Thus, $\boldsymbol{\varepsilon}$ in equation (1) is an error vector comprising the measurement error and *the forward model error*. Our methodology, which is derived based on equation (1), is in principle applicable to the analysis of the forward model error, although in this study we choose not to explicitly analyze this contribution but focus on the measurement error.

The vectors $\boldsymbol{y}$ and $\boldsymbol{\varepsilon}$ both have a dimension m (i.e., m is the total number of measurement elements, e.g., spectral channels). Here $\boldsymbol{x}$ is the state vector to be retrieved, with a dimension n. Following the notation of Multivariate Statistics [e.g., *Anderson*, 2003; *Härdle and Simar*, 2007; *Tabachnick and Fidell*, 2013], if a random vector $\boldsymbol{z}$ has p elements and obeys a multivariate normal (Gaussian) distribution with a mean $\boldsymbol{\mu}$ and a covariance matrix $\boldsymbol{\Sigma}$, this distribution is denoted as $\boldsymbol{z} \sim N_p(\boldsymbol{\mu}, \boldsymbol{\Sigma})$. Typically as a good approximation, the error $\boldsymbol{\varepsilon}$ in equation (1) is commonly assumed to obey the following normal distribution:

$$\boldsymbol{\varepsilon} \sim N_m(0, \boldsymbol{S}_\varepsilon), \tag{2}$$

where $\boldsymbol{S}_\varepsilon$ is the error covariance matrix of the measurement. Our study follows *O'Dell et al*. [2012] and *Bowman et al*. [2002, 2006], by parameterizing the error covariance ($\boldsymbol{S}_\varepsilon$) to be zero-mean and Gaussian diagonal for the convenience of our multivariate statistical analysis. This parameterization certainly does not faithfully represent the forward model uncertainties but is appropriate for the specific purpose of our study. The meanings of all mathematical symbols in this manuscript are listed in Table 1 as an easy/quick reference for the reader.

The measurements and the forward model generally cannot guarantee a unique mapping from $\boldsymbol{x}$ to $\boldsymbol{y}$ or vice versa, partly due to the inevitable uncertainty as represented by $\boldsymbol{\varepsilon}$. Therefore, a simple-minded approach of inverting equation (1) often leads to unphysical solutions [e.g., *Rodgers*, 2000, section 1.3]. To fix this

Table 1. The Meanings of Various Mathematical Symbols for Quick Reference

$\boldsymbol{z} \sim N_P(\boldsymbol{\mu}, \boldsymbol{\Sigma})$	$\boldsymbol{z}$ is a P-element random vector that follows normal/Gaussian distribution with a mean $\boldsymbol{\mu}$ and a covariance $\boldsymbol{\Sigma}$
$\boldsymbol{x}$	the state vector/scalar to be retrieved
$\boldsymbol{y}$	the measurement vector
ε	the measurement error vector
$\boldsymbol{S}_\varepsilon$	the covariance matrix of the measurement error
$\boldsymbol{x_a}$	the a priori mean state for $\boldsymbol{x}$, the best evaluation for $\boldsymbol{x_c}$ before measurements/retrievals
$\boldsymbol{S_a}$	the a priori covariance matrix for $\boldsymbol{x}$, the best evaluation for $\boldsymbol{S_c}$ before measurements/retrievals
$\boldsymbol{K}$	the weighting function matrix
$\hat{\boldsymbol{x}}$	the retrieval solution
$\hat{\boldsymbol{x}} - \boldsymbol{x}$	the deviation of the retrieval solution $\hat{x}$ from the true state $\boldsymbol{x}$, i.e., the retrieval quaility (retrieval error)
$\boldsymbol{x_c}$	the mean of the distribution of true state $\boldsymbol{x}$
$\boldsymbol{S_c}$	the covariance matrix of the distribution of true state $\boldsymbol{x}$
$\hat{\boldsymbol{S}}$	the (posterior) covariance matrix of retrieval quality according to the approximate framework equation (14), expressed by equation (6)
$\hat{\boldsymbol{S}}\left(\boldsymbol{S_a^{-1}S_cS_a^{-1}} + \boldsymbol{K^T S_\varepsilon^{-1} K}\right)\hat{\boldsymbol{S}}$	the (posterior) covariance matrix of retrieval quality according to the rigorous framework equation (13)
$\hat{\boldsymbol{S}}\boldsymbol{S_a^{-1}}(\boldsymbol{x_a} - \boldsymbol{x_c})$	the accuracy of retrieval quality according to the rigorous framework equation (13)
$\boldsymbol{h}$	a vector representing the vertical pressure-weighted averaging

problem, it is crucial to employ some a priori knowledge about the distribution of the state vector $\boldsymbol{x}$, which is commonly described by Gaussian statistics:

$$\boldsymbol{x} \sim N_n(\boldsymbol{x_a}, \boldsymbol{S_a}). \tag{3}$$

Here $\boldsymbol{x_a}$ is the a priori mean state vector, and $\boldsymbol{S_a}$ is the a priori covariance matrix. This a priori distribution provides an important constraint for the retrieval of $\boldsymbol{x}$, in addition to the constraint from the measurements. The OET retrieval solution, denoted as $\hat{\boldsymbol{x}}$, can be derived by iterative steps that seek to minimize the cost function:

$$\chi^2 = [\boldsymbol{y} - \boldsymbol{F}(\boldsymbol{x})]^T \boldsymbol{S}_\varepsilon^{-1} [\boldsymbol{y} - \boldsymbol{F}(\boldsymbol{x})] + (\boldsymbol{x} - \boldsymbol{x_a})^T \boldsymbol{S}_a^{-1} (\boldsymbol{x} - \boldsymbol{x_a}). \tag{4}$$

The weighting function is usually denoted by $\boldsymbol{K} = [K_{i,j}] = [\partial F_i / \partial x_j]$. Using linearization via a Taylor series, *Rodgers* [2000] (see his equations (2.27) and (2.44)) derives the first-order distribution of the optimal solution as below:

$$\boldsymbol{x} \sim N_n\left(\hat{\boldsymbol{x}}, \hat{\boldsymbol{S}}\right), \tag{5}$$

where the terms are expressed by

$$\hat{\boldsymbol{S}} = \left(\boldsymbol{K^T S_\varepsilon^{-1} K} + \boldsymbol{S_a^{-1}}\right)^{-1} \tag{6}$$

and

$$\hat{\boldsymbol{x}} = \hat{\boldsymbol{S}}\boldsymbol{S_a^{-1}}\boldsymbol{x_a} + \hat{\boldsymbol{S}}\boldsymbol{K^T S_\varepsilon^{-1}}\boldsymbol{K}\boldsymbol{x} + \hat{\boldsymbol{S}}\boldsymbol{K^T S_\varepsilon^{-1}}\varepsilon. \tag{7}$$

Here $\hat{\boldsymbol{S}}$ is the retrieval (posterior) covariance matrix and $\hat{\boldsymbol{x}}$ is the retrieval solution. From (7) it is straightforward to obtain the expression for the retrieval quality (retrieval error), i.e., the deviation of the retrieval solution $\hat{\boldsymbol{x}}$ from the true state $\boldsymbol{x}$, as below:

$$\hat{\boldsymbol{x}} - \boldsymbol{x} = \hat{\boldsymbol{S}}\boldsymbol{S_a^{-1}}\boldsymbol{x_a} - \hat{\boldsymbol{S}}\boldsymbol{S_a^{-1}}\boldsymbol{x} + \hat{\boldsymbol{S}}\boldsymbol{K^T S_\varepsilon^{-1}}\varepsilon. \tag{8}$$

Again, Table 1 explains all mathematical symbols in this manuscript as a quick reference for the reader.

Equation (8) is the starting point of our analysis for CO_2 retrieval errors. In section 2 we illustrate the statistical fundamentals that help characterize the mathematical nature of the associated error analysis. We use the related statistical methodology to systematically deliver a rigorous framework of error analysis, the results of which are demonstrated to be consistent with previous studies as shown in the Appendix A. Specifically in section 3, we quantify the potential errors introduced when treating a priori climatology same as the true state. This is a widely applied approximate framework and we compare it with a rigorously derived benchmark framework. By the nature of the problem considered, realistic numerical simulation may have

advantage over remote sensing measurements for our specific purpose. In section 4, we quantify the intrinsic difference and connection of error analysis between the scenario of the sounding for a nonzero-variate CO_2 state and that for a zero-variate CO_2 state. We draw conclusions and discussions in section 5.

2. Fundamentals of Multivariate Statistics

To facilitate the estimation of atmospheric CO_2 fluxes and transport, GHG satellite missions, such as OCO-2 [e.g., *Frankenberg et al*., 2015; *Crisp et al*., 2016], aim to retrieve column-averaged CO_2 dry air mole fraction (Xco_2) with a precision ~1 ppm (part per million) and an accuracy ~0.2 ppm at certain spatial and temporal scales, e.g., for an ~1000 km × 1000 km region (or smaller scalelike 1–100 km) at semimonthly to monthly intervals [*Miller et al*., 2007; *Buchwitz et al*., 2012]. The variability/distribution of the true CO_2 state under these spatial and temporal scales is assumed to obey multivariate Gaussian statistics:

$$\boldsymbol{x} \sim N_n(\boldsymbol{x_c}, \boldsymbol{S_c}), \tag{9}$$

where $\boldsymbol{x_c}$ is the mean and $\boldsymbol{S_c}$ is the covariance of the true CO_2 state distribution (following the notation of *Rodgers and Connor* [2003]). Here Gaussian statistics is a widely used, albeit incomplete assumption (see discussion in *Bowman et al*. [2002], *Kulawik et al*. [2006]). This true state distribution (9) is to be retrieved and is in theory best evaluated by the a priori distribution (3) before measurement. Thus, the a priori provides one constraint for the retrieval, while the measurement provides another constraint such that the retrieval solution $\hat{\boldsymbol{x}}$ (see its expression above equation (14)) typically approaches closer to the true state (9) than the a priori (3) does. But most likely, the retrieval solution $\widehat{\boldsymbol{x}}$ cannot reach the true state: Only when we have *perfect* measurements (i.e., $\boldsymbol{S}_\varepsilon \to 0$), equation (6) becomes $\widehat{\boldsymbol{S}} \sim \left(\boldsymbol{K}^{\boldsymbol{T}}\boldsymbol{S}_\varepsilon^{-1}\boldsymbol{K}\right)^{-1} \to 0$ and it is straightforward to obtain that $\widehat{\boldsymbol{x}} \sim N_n(\boldsymbol{x_c}, \boldsymbol{S_c})$. This means that the retrievals $\hat{\boldsymbol{x}}$ can completely recover the true state (9) only when the measurement errors are zero, which, however, is an unrealistic situation. Therefore, $\boldsymbol{x_c}$ and $\boldsymbol{S_c}$ in *real-world* retrievals are always unknown (again, best evaluated by the a priori $\boldsymbol{x_a}$ and $\boldsymbol{S_a}$ before measurements), although in *numerical simulations* they can be prescribed to be physical ones (as if they are known) for our specific purpose (as in section 3 for our purpose of a rigorous error analysis).

Therefore, the true CO_2 state $\boldsymbol{x}$ and the retrieved CO_2 state $\widehat{\boldsymbol{x}}$ are both variable vectors. The former obeys the distribution (9). The latter, as a function of $\boldsymbol{x}$ and ε as from (7), obeys a distribution determined by (7), (2), and (9). Their difference, i.e., the retrieval quality (retrieval error), $(\widehat{\boldsymbol{x}} - \boldsymbol{x})$ given by (8), is also a variable vector and obeys a certain distribution. Quantifying this distribution of retrieval quality, as we examine in this note, is a vital component for the remote sensing of CO_2 [e.g., *Buchwitz et al*., 2012]. However, this distribution has a *sophisticated* multivariate dependency on (8), (2), and (9), a systematic analysis of which is *difficult* to perform without utilizing Multivariate Statistics [e.g., *Härdle and Simar*, 2007]. An important point of this paper is that a more *realistic* error analysis of CO_2 retrieval should be based on strict Multivariate Statistics. To our knowledge, Multivariate Statistics, due to its complexity, is often not well understood by some OET practitioners, which is a key element that prevents them from achieving a more correct error analysis. Therefore, it is necessary to include a revisit of Multivariate Statistics, which is not new in the community of statistics but is not well recognized in the community of CO_2 remote sensing.

Without loss of generality, let $\boldsymbol{x}$ be a $(n \times 1)$ vector that follows a multivariate normal distribution $\boldsymbol{x} \sim N_n(\overline{\boldsymbol{x}}, \boldsymbol{S})$ and $\boldsymbol{K}$ be a $(m \times n)$ constant matrix. From Theorem 2.4.5 of *Anderson* [2003], $\boldsymbol{Kx}$ is then distributed as

$$\boldsymbol{Kx} \sim N_m\left(\boldsymbol{K}\overline{\boldsymbol{x}}, \boldsymbol{KSK}^T\right). \tag{10a}$$

This theorem tells us that multivariate normality is preserved under any linear transformations. See *Anderson* [2003] for the proof of this theorem.

As an extension of the theorem (10a), let $\boldsymbol{c}$ be a $(m \times 1)$ constant vector. From Theorem 5.2 of *Härdle and Simar* [2007], $\boldsymbol{Kx} + \boldsymbol{c}$ is distributed as

$$\boldsymbol{Kx} + \boldsymbol{c} \sim N_m\left(\boldsymbol{K}\overline{\boldsymbol{x}} + \boldsymbol{c}, \boldsymbol{KSK}^T\right). \tag{10b}$$

This theorem tells us that if $\boldsymbol{x}$ is distributed according to a multivariate normal statistics, then every linear function of $\boldsymbol{x}$ should consistently follow a normal distribution as well.

Next, let $\boldsymbol{x}$ and $\boldsymbol{y}$ both be $(n\times 1)$ dimensional vectors, each distributed independently as $\boldsymbol{x}\sim N_n(\overline{\boldsymbol{x}},\boldsymbol{S_x})$ and $\boldsymbol{y}\sim N_n(\overline{\boldsymbol{y}},\boldsymbol{S_y})$. From Theorem 2.19 of *Basilevsky* [1994], $(\boldsymbol{x}+\boldsymbol{y})$ should be distributed according to

$$(\boldsymbol{x}+\boldsymbol{y})\sim N_n(\overline{\boldsymbol{x}}+\overline{\boldsymbol{y}},\boldsymbol{S_x}+\boldsymbol{S_y}). \tag{11a}$$

This theorem tells us that adding two independent Gaussian distribution yields another Gaussian distribution.

Finally, as an extension of the theorem (11a), let $\boldsymbol{x_1}, \boldsymbol{x_2}, \ldots, \boldsymbol{x_I}$ be independently, identically distributed vectors according to $N_n(\bar{\boldsymbol{x}}, \boldsymbol{S})$. Let $\sum_{i=1}^{I}\frac{\boldsymbol{x_i}}{I}$ be the sample mean vector. Then from Theorem 3.5.2 of *Tong* [1990], $\sum_{i=1}^{I}\frac{\boldsymbol{x_i}}{I}$ obeys the following multivariate normal distribution:

$$\sum_{i=1}^{I}\frac{\boldsymbol{x_i}}{I}\sim N_n(\overline{\boldsymbol{x}},\ \boldsymbol{S}/I). \tag{11b}$$

This theorem tells us that multiple sampling would reduce the covariance uncertainty by a factor of the sample number (i.e., reduce $\boldsymbol{S}$ to be $\boldsymbol{S}/I$).

Now we utilize the statistical fundamentals above to analyze the properties of the retrieval quality (retrieval error) $(\widehat{\boldsymbol{x}}-\boldsymbol{x})$, as given by equation (8). There are three controlling terms on the right-hand side (RHS) of (8). The first term $\widehat{\boldsymbol{S}}\boldsymbol{S_a}^{-1}\boldsymbol{x_a}$ is a constant vector and hence has a zero covariance, i.e.,

$$\widehat{\boldsymbol{S}}\boldsymbol{S_a}^{-1}\boldsymbol{x_a}\sim N_n\left(\widehat{\boldsymbol{S}}\boldsymbol{S_a}^{-1}\boldsymbol{x_a},\ 0\right). \tag{12a}$$

In contrast, the second term $-\widehat{\boldsymbol{S}}\boldsymbol{S_a}^{-1}\boldsymbol{x}$ and the third term $\widehat{\boldsymbol{S}}\boldsymbol{K}^{\boldsymbol{T}}\boldsymbol{S_\varepsilon}^{-1}\varepsilon$ are both variable vectors. They are a linear function of $\boldsymbol{x}$ and ε, respectively. Therefore, we can apply (2), (9), and (10a) to achieve their multivariate normal distribution:

$$-\widehat{\boldsymbol{S}}\boldsymbol{S_a}^{-1}\boldsymbol{x}\sim N_n\left(-\widehat{\boldsymbol{S}}\boldsymbol{S_a}^{-1}\boldsymbol{x_c},\ \ \widehat{\boldsymbol{S}}\boldsymbol{S_a}^{-1}\boldsymbol{S_c}\boldsymbol{S_a}^{-1}\widehat{\boldsymbol{S}}\right), \tag{12b}$$

$$\widehat{\boldsymbol{S}}\boldsymbol{K}^{T}\boldsymbol{S_\varepsilon}^{-1}\varepsilon\sim N_n\left(0,\ \widehat{\boldsymbol{S}}\boldsymbol{K}^{T}\boldsymbol{S_\varepsilon}^{-1}\boldsymbol{K}\widehat{\boldsymbol{S}}\right). \tag{12c}$$

Finally, according to (11a), the linear combination of (12a)–(12c), due to their independence, leads to the following multivariate normal distribution for the retrieval quality (retrieval error):

$$(\widehat{\boldsymbol{x}}-\boldsymbol{x})\sim N_n\left(\widehat{\boldsymbol{S}}\boldsymbol{S_a}^{-1}(\boldsymbol{x_a}-\boldsymbol{x_c})\right),\ \widehat{\boldsymbol{S}}\left(\boldsymbol{S_a}^{-1}\boldsymbol{S_c}\boldsymbol{S_a}^{-1}+\boldsymbol{K}^{T}\boldsymbol{S_\varepsilon}^{-1}\boldsymbol{K}\right)\widehat{\boldsymbol{S}}). \tag{13}$$

Here the mean $\widehat{\boldsymbol{S}}\boldsymbol{S_a}^{-1}(\boldsymbol{x_a}-\boldsymbol{x_c})$ represents the *accuracy* of the retrieval quality: the statistical *bias* of the retrieval solution $\widehat{\boldsymbol{x}}$ from the true state $\boldsymbol{x}$ (accuracy is often called bias in the literature). The covariance $\widehat{\boldsymbol{S}}\left(\boldsymbol{S_a}^{-1}\boldsymbol{S_c}\boldsymbol{S_a}^{-1}+\boldsymbol{K}^{\boldsymbol{T}}\boldsymbol{S_\varepsilon}^{-1}\boldsymbol{K}\right)\widehat{\boldsymbol{S}}$ represents the precision (statistical variability) of the retrieval quality (see *Taylor* [1999] for a rigorous statistical definition of accuracy and precision).

Therefore, we have applied the methodology of Multivariate Statistics to systematically obtain the rigorous framework (13). Our Appendix A demonstrates the consistency of our equation (13) with previous studies for a *rigorous* error analysis of OET, by also applying the statistical methodology. This methodology is a useful tool in performing error analysis for various retrieval scenarios, as further shown in the rest of this manuscript.

The statistical nature of the retrieval quality using OET is essentially captured by equation (13), whose physical meaning is not straightforward. Figure 1a schematically illustrates the physical meaning of (13) in a simple scenario of a two-dimensional state vector ($\boldsymbol{x}=[x_1, x_2]$) and a one-dimensional measurement ($\boldsymbol{y}$). This schematic essentially follows Figure 2.4 of *Rodgers* [2000] but now adds the effects of $\boldsymbol{x_c}$ and $\boldsymbol{S_c}$. The golden ellipse represents the variability/distribution of the true state $\boldsymbol{x}$, which is shown within the range of the covariance $\boldsymbol{S_c}$ with the mean $\boldsymbol{x_c}$ at the center (i.e., $\boldsymbol{x}\sim N_n(\boldsymbol{x_c}, \boldsymbol{S_c})$, equation (9)). To retrieve $\boldsymbol{x}$ via a Bayesian approach, there should be two constraints. The first constraint is the a priori knowledge/guess about the true state's distribution: $\boldsymbol{x}\sim N_n(\boldsymbol{x_a}, \boldsymbol{S_a})$ (equation (3)), as represented by the purple ellipse. The second constraint of $\boldsymbol{x}$ comes from the measurement, as represented by the green region. (That is, given the measurement $\boldsymbol{y}$ and the weighting function $\boldsymbol{K}$, the Gaussian uncertainty of the measurement error ε leads to the variability of $\boldsymbol{x}$ shown by the green region, as directly inversed from the first-order expression for the forward model $\boldsymbol{y}=\boldsymbol{K}\boldsymbol{x}+\varepsilon$.) The

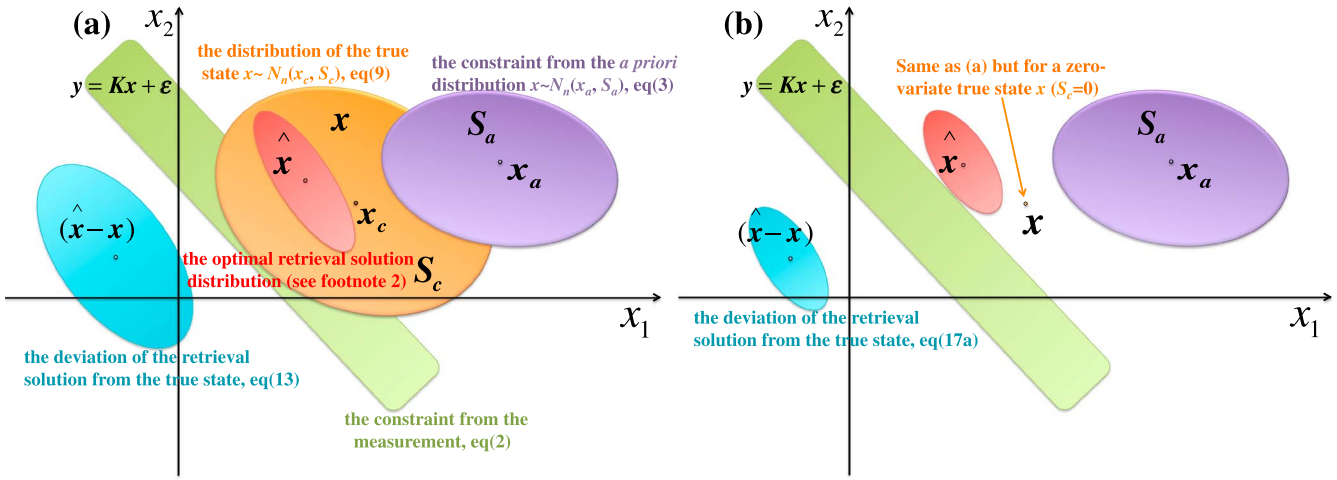

Figure 1. (a) Schematic for the physical meaning of equation (13), for the scenario of a two-dimensional CO_2 state vector and a one-dimensional measurement, as discussed in sections 2-3. This schematic essentially follows Figure 2.4 of *Rodgers* [2000], but now adds the effects of $\boldsymbol{x_c}$ and $\boldsymbol{S_c}$. The golden ellipse represents the variability/distribution of the true state $\boldsymbol{x}$, which is shown within the range of the covariance $\boldsymbol{S_c}$ with the mean $\boldsymbol{x_c}$ at the center [i.e., $\boldsymbol{x} \sim N_n(\boldsymbol{x_c}, \boldsymbol{S_c})$]. The first constraint for the retrieval is the a priori knowledge $\boldsymbol{x} \sim N_n(\boldsymbol{x_a}, \boldsymbol{S_a})$, as represented by the purple ellipse. The second constraint for the retrieval comes from the measurement, as represented by the green region. The Bayesian statistics combines the above two constraints sophisticatedly to result in the optimal solution $\hat{\boldsymbol{x}}$ with a smaller uncertainty than either of the two constraints, as represented by the red ellipse. Finally, the blue ellipse represents the uncertainty of the retrieval quality ($\hat{\boldsymbol{x}} - \boldsymbol{x}$), as quantified by (13). (b) Same as (a) but for the scenario of a zero-variate true CO_2 state $\boldsymbol{x}$, i.e., a single data point ($\boldsymbol{S_c} = 0$), as discussed in section 4. The distribution of ($\hat{\boldsymbol{x}} - \boldsymbol{x}$) here is according to equation (17a).

Bayesian statistics combines the above two constraints to yield the optimal solution $\hat{\boldsymbol{x}}$ with a *smaller* uncertainty than either of the two constraints, as represented by the red ellipse. (From (7), (10a), (10b), and (11a), we can obtain the variability/distribution of $\hat{\boldsymbol{x}} \sim N_n(\hat{\boldsymbol{S}}\boldsymbol{S_a}^{-1}\boldsymbol{x_a} + \hat{\boldsymbol{S}}\boldsymbol{K}^T\boldsymbol{S_\varepsilon}^{-1}\boldsymbol{K}\boldsymbol{x_c}, \hat{\boldsymbol{S}}\boldsymbol{K}^T\boldsymbol{S_\varepsilon}^{-1}\boldsymbol{K}(\boldsymbol{S_c}\boldsymbol{K}^T\boldsymbol{S_\varepsilon}^{-1}\boldsymbol{K} + 1)\hat{\boldsymbol{S}})$, as represented by the red ellipse.) Finally, the blue ellipse represents the uncertainty of the retrieval quality ($\hat{\boldsymbol{x}} - \boldsymbol{x}$), as characterized by equation (13).

Equation (13) is a rigorous representation for the retrieval quality (again, see the Appendix A). Note, however, that this representation also has limitations, e.g., not accounting for the non-Gaussian effect. At least partly due to the reasons discussed below, numerous previous studies have widely applied the following *approximate* framework for the error analysis of CO_2 retrieval [e.g., *O' Dell et al.*, 2012; *Bovensmann et al.*, 2010; *Bösch et al.*, 2006; *Boesch et al.*, 2011; *Yoshida et al.*, 2011; *Reuter et al.*, 2010], implicitly or explicitly, as detailed right above equation (16) in section 3:

$$(\hat{\boldsymbol{x}} - \boldsymbol{x}) \sim N_n\left(0, \hat{\boldsymbol{S}}\right). \tag{14}$$

The key assumption in (14) is to approximate the true state distribution $\boldsymbol{x} \sim N_n(\boldsymbol{x_c}, \boldsymbol{S_c})$ by the a priori distribution $\boldsymbol{x} \sim N_n(\boldsymbol{x_a}, \boldsymbol{S_a})$: i.e., using $\boldsymbol{x_c} = \boldsymbol{x_a}$ and $\boldsymbol{S_c} = \boldsymbol{S_a}$ in the rigorous framework, equation (13) yields the approximate one (14).

The approximation equation (14) is still useful due to the following reasons. The to-be-retrieved true-state distribution, $\boldsymbol{x} \sim N_n(\boldsymbol{x_c}, \boldsymbol{S_c})$, is by definition *impossible* to know precisely in advance of retrievals except in numerical experiments (see more discussions in the beginning of section 2) [see also *Eguchi et al.*, 2010]. Thus, equation (13), which includes the unknown parameters $\boldsymbol{x_c}$ and $\boldsymbol{S_c}$, cannot be applied directly. Again, in theory, the best evaluation for ($\boldsymbol{x_c}$, $\boldsymbol{S_c}$) before measurements should be the a priori knowledge ($\boldsymbol{x_a}$, $\boldsymbol{S_a}$), which is known. Thus, in this sense it is reasonable to approximate ($\boldsymbol{x_c}$, $\boldsymbol{S_c}$) by ($\boldsymbol{x_a}$, $\boldsymbol{S_a}$) in the rigorous framework equation (13), which yields the approximation equation (14) that is determinable in real-world retrievals. However, even though equation (14) is practically useful, this does not change the fact that it is an approximate framework and it can cause *error* when evaluating the precision and accuracy (i.e., equation (13) does not equal equation (14) if ($\boldsymbol{x_a}$, $\boldsymbol{S_a}$) differs from ($\boldsymbol{x_c}$, $\boldsymbol{S_c}$), no matter how small this difference is). Therefore, the follow-up question is whether this error is negligible or nonnegligible for CO_2 retrievals. To answer this question, in many aspects it is actually advantageous to use numerical simulations rather than real-world remote sensing measurements. This is essentially because, again, the

true state ($\boldsymbol{x_c}$, $\boldsymbol{S_c}$) is not known in real-world retrievals but can be prescribed as if it is known in numerical simulation, as we do in this study. Of course, $\boldsymbol{x_c}$ and $\boldsymbol{S_c}$ should be prescribed to be as physical/realistic as possible, as we attempt to do in section 3. This manuscript aims to explore this issue self-consistently using the statistical methodology and hopefully shed some light on the question raised above. But it is never intended to be an exhaustive study on this issue, due to the complicated and extensive variability of true CO_2 profile state in reality [see, e.g., *Eguchi et al*., 2010; *Zeng et al*., 2012, 2014]. Our study should also *not* be considered as a criticism to the usage of equation (14), which is a practical framework as discussed above. Again, the reader may also refer to other literature that mentions/discusses the similar issue but with different focuses [e.g., *Kulawik et al*., 2006; *O'Dell et al*., 2012; *Worden et al*., 2004; *Connor et al*., 2008; *Reuter et al*., 2012; *Cressie et al*., 2016; *Connor et al*., 2016].

3. Numerical Illustrations

Here we examine the potential discrepancy between the approximate framework (14) and the more rigorous framework (13) in the error analysis of CO_2 retrieval. Here we use the OCO orbit simulator, whose model configurations are detailed in *O'Brien et al*. [2009]. For the purpose of this work, we only consider the clear-sky scenario, whose fraction among the global observations is about 15% under OCO-2 2 km^2 spatial resolution [*Miller et al*., 2007]. Without loss of generality, the configured atmosphere is composed of 11 layers; the measurement $\boldsymbol{y}$ includes 500 spectrally resolved radiances from 6167.7 to 6220.9 cm^{-1} spectra (i.e., using the 1.6 μm CO_2 band, with a OCO-2 resolution ~0.1 cm^{-1}, equally spaced) [see *Kuai et al*., 2010]. The quantity of interest, Xco_2, can be calculated as $\boldsymbol{h^T x}$, where $\boldsymbol{x}$ is the state vector representing the vertical profile of CO_2 (i.e., with 11 layers here) and $\boldsymbol{h}$ is a vector representing the vertical pressure-weighted averaging. From (13) and the statistical fundamental (10a), we obtain the univariate normal distribution for the Xco_2 retrieval quality (the deviation of the retrieval from the true state):

$$\left(\boldsymbol{h^T\hat{x}} - \boldsymbol{h^T x}\right) \sim \boldsymbol{N}_1\left(\boldsymbol{h^T\hat{S}S_a^{-1}}(\boldsymbol{x_a} - \boldsymbol{x_c}), \boldsymbol{h^T\hat{S}}\left(\boldsymbol{S_a^{-1}S_cS_a^{-1}} + \boldsymbol{K^TS_\varepsilon^{-1}K}\right)\boldsymbol{\hat{S}h}\right). \tag{15}$$

From fundamental statistics [e.g., *Anderson*, 2003], the first term and the second term in the RHS of (15), respectively, represent the accuracy and the variance (the square of precision) of the Xco_2 retrieval quality. In contrast to (15), a widely applied approximate framework for the distribution of the Xco_2 retrieval quality, explicitly or implicitly [e.g., *O' Dell et al*., 2012, equation (B3); *Bovensmann et al*., 2010, equation (B16); *Boesch et al*., 2011, equation (5); *Bösch et al*., 2006, equation (6); *Yoshida et al*., 2011, equation (12); *Reuter et al*., 2010, equation (12)], is represented as follows:

$$\left(\boldsymbol{h^T\hat{x}} - \boldsymbol{h^T x}\right) \sim N_1\left(0, \boldsymbol{h^T\hat{S}h}\right). \tag{16}$$

We note that equation (15) becomes equation (16) only when assuming $\boldsymbol{x_c} = \boldsymbol{x_a}$ and $\boldsymbol{S_c} = \boldsymbol{S_a}$, which is the same simplifying assumption that produces equation (14) from equation (13). This is because (16) and (15) are the linear transformations of (14) and (13), respectively, by utilizing the statistical fundamental (10a).

The approximate framework (16) yields a perfect accuracy (i.e., zero bias). In contrast, the more rigorous framework (15) generally yields nonzero accuracy: $\boldsymbol{h^T\hat{S}S_a^{-1}}(\boldsymbol{x_a} - \boldsymbol{x_c})$. Here $(\boldsymbol{x_a} - \boldsymbol{x_c})$ is the deviation of the a priori CO_2 profile (i.e., $\boldsymbol{x_a}$) from the true profile (i.e., $\boldsymbol{x}_c$), representing the bias of our best knowledge for the true state before the measurement/retrieval. According to *Eguchi et al*. [2010], our current best knowledge of CO_2 profile has a bias of about 3.2–7.2 ppm on average [see some recent values in *Wunch et al*., 2016], resulting from the complexity of the often-chaotic climate variability that is currently not well predicted/measured [e.g., *Jiang et al*., 2010, 2016].

Now we numerically examine the potential error introduced when evaluating the accuracy of Xco_2 retrieval quality using the approximate framework (16), in contrast to the rigorous framework (15). As discussed at the end of section 2, the true state ($\boldsymbol{x_c}$, $\boldsymbol{S_c}$) is actually unknown and is best evaluated by ($\boldsymbol{x_a}$, $\boldsymbol{S_a}$) before our measurements. Therefore, by definition in *real-world* retrievals, we generally cannot determine $(\boldsymbol{x_a} - \boldsymbol{x_c})$ accurately (since $\boldsymbol{x}_c$ is unknown), but we can prescribe it in numerical simulations where $(\boldsymbol{x_a} - \boldsymbol{x_c})$ represents the uncertainty/bias of our knowledge for the true state before our retrievals. To be physical and without loss of generality, in our experiments we configure some statistically significant structures for the vertical profile of $(\boldsymbol{x_a} - \boldsymbol{x_c})$: constant, linear,

Table 2. Configurations of Four Numerical Cases That Contrast the Accuracy of Xco_2 Retrieval Quality ($\hat{x} - x$) According to the Rigorous Framework (15) and the Approximate Framework (16), With Results Discussed in Figure 2 and Section 3[a]

	x_a
Case 1	$x_a(i) = x_c(i) + 3.2$ ppm
Case 2	$x_a(i) = x_c(i) + 1.6$ ppm $\times$ [1–2(i − 1)/10]
Case 3	$x_a(i) = x_c(i) + 1.6$ ppm $\times$ [((i − 1)/10 − 3/2)^2 − 5/4]
Case 4	$x_a(i) = x_c(i) + 1.6$ ppm $\times$ [((i − 1)/10 + 0.264)^3 − 1.018]

[a]By definition $(x_a - x_c)$ in real-world retrievals can not be determined exactly (detailed in section 3). But as numerical experiments we can prescribe the vertical profile of $(x_a - x_c)$ to be some statistically/physically significant structures: constant, linear, quadratic, and cubic, in the four cases respectively. The uncertainty magnitude of $(x_a - x_c)$ is configured to be $\lesssim$3.2 ppm according to *Eguchi et al.* [2010]. The S_a in all four cases is diagonal matrices with diagonal elements of 8 ppm, which is a typical a priori magnitude for many realistic retrievals of Xco_2 [e.g., *Kuang et al.*, 2002 use 8 ppm; *Saitoh et al.*, 2009 use 10 ppm]. Here i ($i = 1, 2, \ldots, 11$) is the index for the vertical layers in the model.

quadratic, and cubic, respectively. The configurations are detailed in Table 2. The uncertainty magnitude of $(x_a - x_c)$ is configured to be $\lesssim$3.2 ppm following *Eguchi et al.* [2010] [see also *Keppel-Aleks et al.*, 2011, Table 1]. The S_a in all four cases are configured as diagonal matrices [e.g., *Saitoh et al.*, 2009] with diagonal elements of 8 ppm, a typical a priori magnitude for many realistic retrievals of Xco_2 (e.g., *Kuang et al.* [2002] use 8 ppm and *Saitoh et al.* [2009] use 10 ppm). Note that *Saitoh et al.* [2009] obtain improved retrievals when using prescribed diagonal elements for S_a like 10 ppm than when using more constrained values as determined by CO_2 transport model outputs.

Our results are shown in Figure 2. The accuracy of Xco_2 retrieval quality according to the approximate framework (16) is zero in all cases. In contrast, according to the more rigorous framework (15), the true accuracy in these four cases are ~0.19 ppm, ~0.25 ppm, ~0.28 ppm, and ~0.17 ppm, respectively, at SNR = 400 (i.e., the SNR magnitude for OCO-2). The large variability here (from 0.17 to 0.28 ppm) suggests a high sensitivity of the accuracy of Xco_2 retrieval to the vertical structure of the difference between a priori profile and the true profile of CO_2 (due to a vertical dependence according to equation (15)). This 0.17–0.28 ppm accuracy error is non-negligible, by noting that the current GHG-CCI (GreenHouse Gas-Climate Change Initiative) project by ESA aims

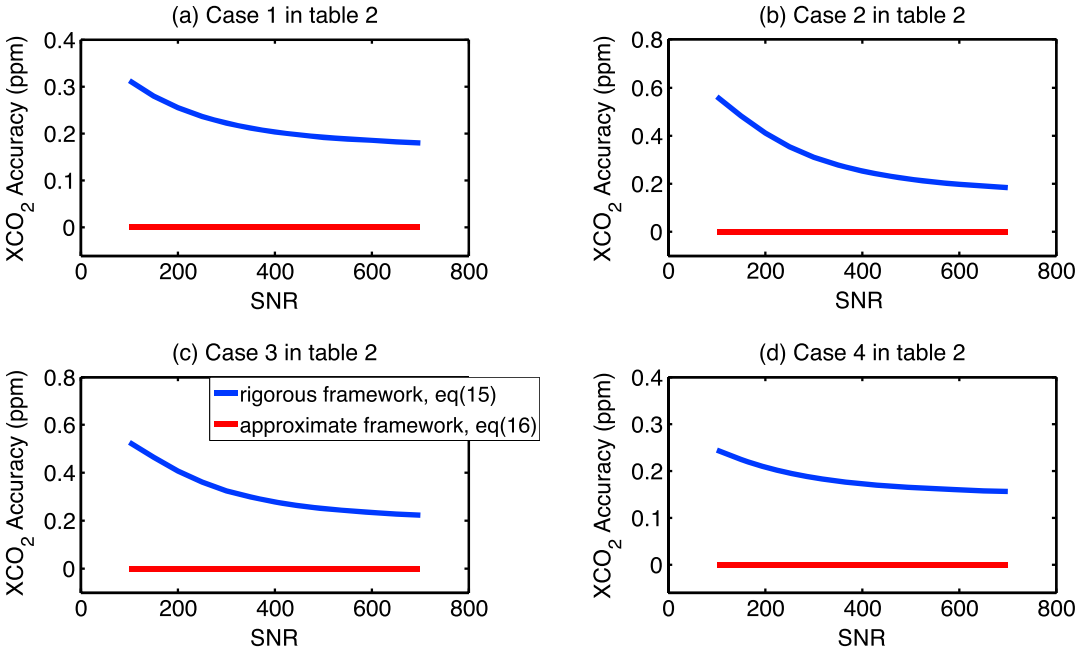

Figure 2. Four numerical cases that illustrate the accuracy of Xco_2 retrieval quality ($h^T \hat{x} - h^T x$), vs SNR. The red curve (always zero) is according to the approximate framework (16). In contrast, the blue curve is according to the more rigorous framework (15). Here the configurations include an uncertainty vector $(x_a - x_c)$ according to some statistically significant vertical structures: constant, linear, quadratic, and cubic, in the four cases respectively. The magnitude of $(x_a - x_c)$ and S_a are configured as detailed in Table 2. This figure shows that the accuracy difference between the two curves is nonnegligible, ~0.17–0.28 ppm at SNR = 400 for these four cases.

Table 3. Configurations of Four Numerical Cases That Contrast the Precision of Xco_2 Retrieval Quality ($\hat{\boldsymbol{x}} - \boldsymbol{x}$) According to the Rigorous Framework (15) and the Approximate Framework (16), With Results Discussed in Figure 3 and Section 3[a]

	$\boldsymbol{S_a}$	$\boldsymbol{S_c}$
Case 1	$(\boldsymbol{S_a})_{i,j} = (8\ \text{ppm})^2 \times \exp(-\lvert i - j\rvert/10)$	$(\boldsymbol{S_c})_{i,j} = (12\ \text{ppm})^2 \times \exp(-\lvert i - j\rvert^2/10)$
Case 2	$(\boldsymbol{S_a})_{i,i} = (8\ \text{ppm})^2$ diagonal	$(\boldsymbol{S_c})_{i,j} = (12\ \text{ppm})^2 \times \exp(-\lvert i - j\rvert/10)$
Case 3	$(\boldsymbol{S_a})_{i,i} = (8\ \text{ppm})^2$ diagonal	$(\boldsymbol{S_c})_{i,j} = (12\ \text{ppm})^2 \times \exp(-\lvert i - j\rvert^2/10)$
Case 4	$(\boldsymbol{S_a})_{i,j} = (20\ \text{ppm})^2 \times \exp(-\lvert i - j\rvert/10)$	$(\boldsymbol{S_c})_{i,j} = (12\ \text{ppm})^2 \times \exp(-\lvert i - j\rvert^2/10)$

[a]The diagonal elements of $\boldsymbol{S_a}$ and $\boldsymbol{S_c}$ can differ by ~3.2–7.2 ppm [*Eguchi et al*., 2010]. This difference in cases 1–3 is configured to be 4 ppm [i.e., 8 ppm for $\boldsymbol{S_a}$ and 12 ppm for $\boldsymbol{S_c}$]. Further, the off-diagonal structure of $\boldsymbol{S_a}$ may considerably deviate from that of $\boldsymbol{S_c}$ due to the hard-to-predict nonlocal dynamics [*Saitoh et al*., 2009]. Therefore these off-diagonal structures here are prescribed based on previous studies: a zero off-diagonal structure [*Saitoh et al*., 2009; *Kuang et al*., 2002], the structure of $\exp(-|i-j|/10)$ [section 2.6 of *Rodgers*, 2000], and the structure of $\exp(-|i-j|^2/10)$ [according to the principle of *Saitoh et al*. [2009] that the correlations between layers should become weaker quickly with increasing distance between the layers]. Case 4 is designed to answer the question of to what degree should the diagonal elements of $\boldsymbol{S_a}$ and $\boldsymbol{S_c}$ be different in order to compensating their off-diagonal inequality for reaching the same precision when using (15) and (16). Here i and j (i, $j = 1, 2, \ldots, 11$) are the indexes for the vertical layers in the model.

to deliver space-based Xco_2 retrieval with an accuracy $\lesssim$0.2 ppm [*Buchwitz et al*., 2012]. Note that the numerical experiments here are essentially a best case scenario and retrievals with real data will likely yield a larger bias.

Next, we examine the potential error introduced when evaluating the *precision* of Xco_2 retrieval quality using the approximate framework (16), in contrast to the benchmark (15). If the a priori covariance $\boldsymbol{S_a}$ differs from the true covariance $\boldsymbol{S_c}$, the approximate precision (variance) term $\boldsymbol{h^T \hat{S} h}$, as in (16), would deviate from the rigorous precision term $\boldsymbol{h^T \hat{S}\left(S_a^{-1} S_c S_a^{-1} + K^T S_\varepsilon^{-1} K\right)\hat{S}h}$ as in (15). As discussed before, by definition in real-world retrievals we cannot determine ($\boldsymbol{S_a} - \boldsymbol{S_c}$) exactly, although *numerically* we can (as in this study). Our numerical experiments here use some prescribed parameterizations for the difference between $\boldsymbol{S_a}$ and $\boldsymbol{S_c}$, based on several studies, with details below. Following *Eguchi et al*. [2010], the standard deviation (diagonal elements) of $\boldsymbol{S_a}$ and $\boldsymbol{S_c}$ is configured to be 4 ppm in cases 1–3 of our new experiments (Table 3; 8 ppm for $\boldsymbol{S_a}$ and 12 ppm for $\boldsymbol{S_c}$; note that ~10 ppm diagonal elements for $\boldsymbol{S_a}$ yield good retrievals in *Saitoh et al*. [2009]). Further, the off-diagonal structure of $\boldsymbol{S_c}$ is related to complicated nonlocal dynamics and is difficult to characterize well by $\boldsymbol{S_a}$ [*Saitoh et al*., 2009]: i.e., the structure of $\boldsymbol{S_a}$ can considerably deviate from $\boldsymbol{S_c}$. These off-diagonal structures in our cases (Table 3) are parameterized by a zero off-diagonal structure [*Saitoh et al*., 2009], the structure of $\exp(-|i-j|/10)$ (section 2.6 of *Rodgers* [2000], here i, j are the indexes for vertical layers], and the structure of $\exp(-|i-j|^2/10)$ [according to the principle of *Saitoh* [2009] that the correlations between layers should become weaker quickly with increasing distance between the layers].

As shown in Figures 3a–3c, the precision differences [when using (16) vs (15)] in cases 1–3 are ~1.4–1.7 ppm at SNR = 400 (the SNR magnitude for OCO-2). This represents the error introduced by using the approximate framework (16) in opposition to the rigorous one (15). This 1.4–1.7 ppm precision error is nonnegligible since the precision goal is $\lesssim$1 ppm for the GHG-CCI project regarding the Xco_2 retrieval [*Buchwitz et al*., 2012]. Case 4 in Table 3 and Figure 3d is designed to answer the question of to what degree should the diagonal elements of $\boldsymbol{S_a}$ and $\boldsymbol{S_c}$ be different in order to compensate their off-diagonal inequality for reaching the same precision when using (15) vs (16) (i.e., the two curves in Figure 3d are close to each other). To test this, we configure $\boldsymbol{S_a}$ and $\boldsymbol{S_c}$ with *unrealistic* large differences (~20 ppm vs 12 ppm, as shown in Case 4 of Table 3) in their diagonal elements. This suggests that it is generally difficult to make the precision difference between (15) and (16) vanish. Again our test cases here are somewhat idealized since the true state distribution/variability can often be complicated [e.g., *Zeng et al*., 2012, 2014] and the difference between $\boldsymbol{S_a}$ and $\boldsymbol{S_c}$ is poorly quantified [*Eguchi et al*., 2010]. Further, in real-world retrievals the framework equation (16) is still useful due to the uncertainty of the true state ($\boldsymbol{S_c}$, $\boldsymbol{x_c}$) in reality. But for numerical simulation (as in this study), equation (15) can act as a valuable benchmark since the true state is then prescribed. Similarly if highly accurate in situ measurements are available, equation (15) can act as a useful benchmark for remote sensing retrievals since the true state is then known.

Note that all discussions above are based on single sounding (for a Gaussian-variate true state), which is an important remote sensing scenario [e.g., *Buchwitz et al*., 2012; *Reuter et al*., 2011]. Another important scenario is multiple soundings: e.g., consider l soundings of CO_2 that are nearly independently and identically

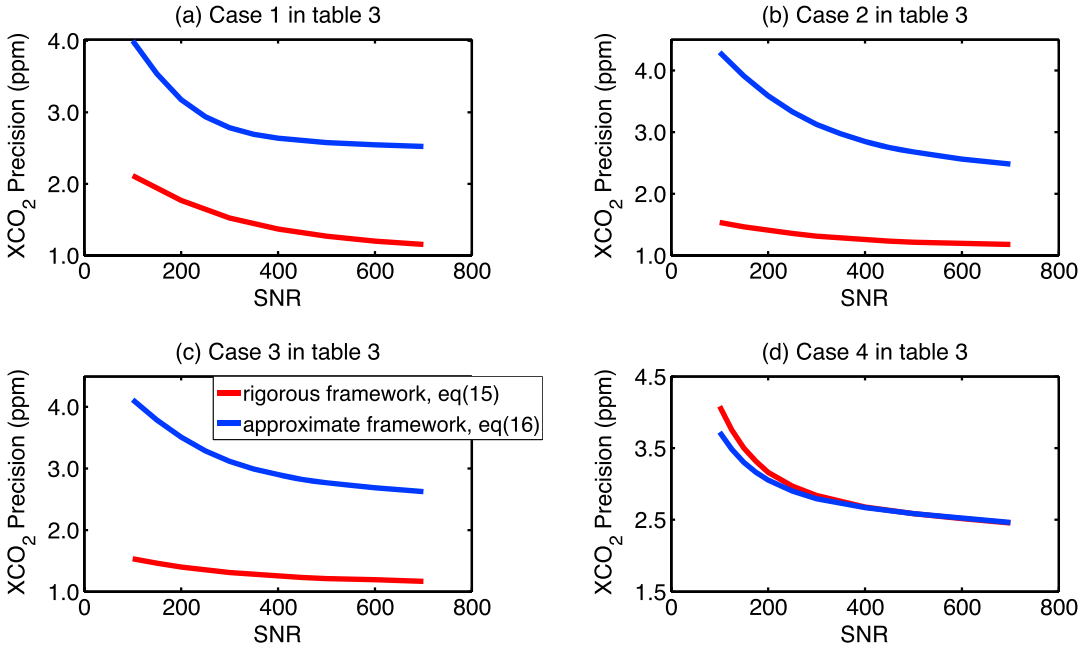

Figure 3. Four numerical cases that illustrate the precision of Xco_2 retrieval quality ($\boldsymbol{h}^T\hat{\boldsymbol{x}} - \boldsymbol{h}^T\boldsymbol{x}$), vs SNR. The red curve is according to the approximate framework (16). In contrast, the blue curve is according to the more rigorous framework (15). The diagonal elements of $\boldsymbol{S_a}$ and $\boldsymbol{S_c}$ is configured as 4 ppm in cases 1–3. Their off-diagonal structures here are parameterized as detailed in Table 3. Case 4 in Table 3 is designed to answer the question of to what degree should the diagonal elements of $\boldsymbol{S_a}$ and $\boldsymbol{S_c}$ be different in order to compensating their off-diagonal inequality for reaching the same precision when using (15) and (16). In panels (a)–(c), the precision difference between the two curves is ~1.4–1.7 ppm at SNR = 400, which is nonnegligible.

distributed (i.e., within the examined spatial and temporal variabilities), with the caveat that Xco_2 retrievals in reality are never entirely independent from each other [*Kulawik et al.*, 2016; *Hammerling et al.*, 2012]. According to the statistical fundamental (11b), the sample mean of multiple sounding (assume I soundings) of Xco_2 retrievals would yield a retrieval quality that is similar to the single-sounding scenario: it can be quantified rigorously by (15) or approximately by (16), except that the variance term should now be divided by a factor of I in both frameworks. This is consistent with Figure 4 of *Kuang et al.* [2002]. (The variance decreases with the sounding number by a factor of I. Therefore, the precision, which is the square root of the variance, is improved with the sounding number by a factor of $I^{0.5}$.) Therefore, all conclusions/comparisons above in principle can be similarly applied to the multiple-sounding scenario.

4. The Scenario for a Zero-Variate True State

Sections 2–3 above focus on the retrieval where the true CO_2 state of interest is one defined under a specified spatial-temporal scale/range, e.g., define the true state as the CO_2 for a 1000 km × 1000 km region during February. Therefore, this true state has a variability. Each single sounding measures a sample of the true state; sufficient large amounts of samples may reflect the variability of the defined true state. Therefore, the true state here obeys a certain spatial-temporal variability/distribution that is characterized by a nonzero covariance $\boldsymbol{S_c}$ shown in (9). This is the widely considered scenario [e.g., *Miller et al.*, 2007]. Another important scenario, as considered in this section, is that the true CO_2 state of interest is one defined for a *particular* time and location (i.e., a *single* state at the time/location of the sounding) [e.g., *Wunch et al.*, 2011; *Fu et al.*, 2014]. Therefore, this kind of true state does not have any spatial-temporal variability, i.e., zero-variate as characterized by a zero covariance $\boldsymbol{S_c}$. This definition-related analysis is helpful for snapshot-measurement event, e.g., it is useful to detect local abnormal (non-Gaussian with time/location) sources/sinks of CO_2 or other GHG [e.g., *Kuai et al.*, 2012; *Su et al.*, 2015; *Jiang et al.*, 2013]. In contrast, the framework in sections 2-3 does not work for this non-Gaussian situation since it requires a Gaussian statistics for the true state.

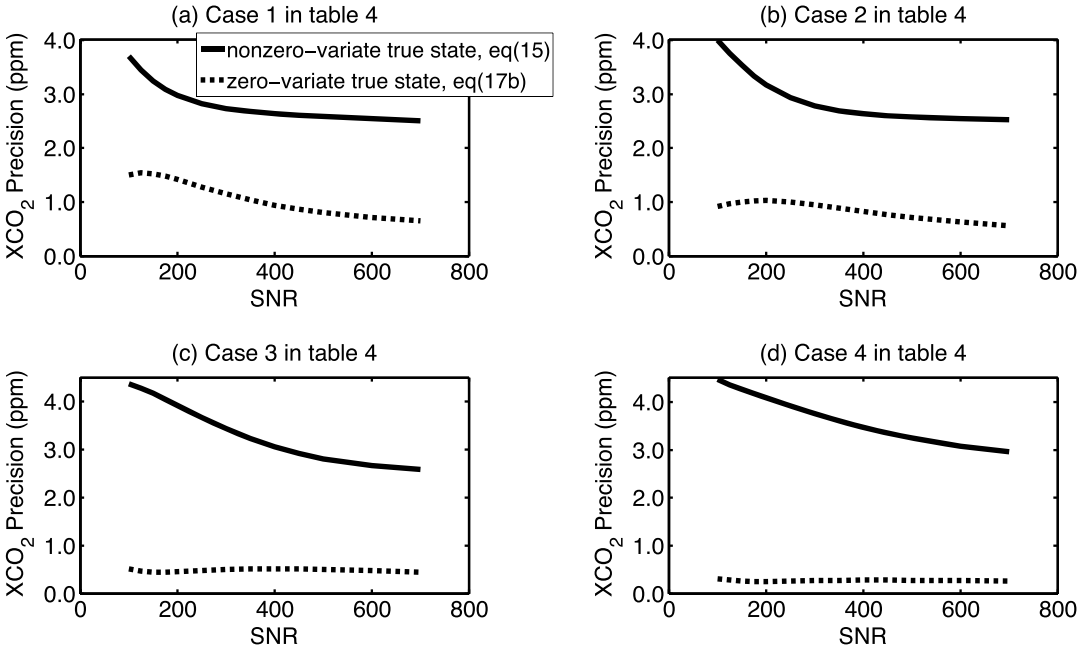

Figure 4. Four numerical cases that illustrate the precision of Xco_2 retrieval quality ($\boldsymbol{h}^T\hat{\boldsymbol{x}} - \boldsymbol{h}^T\boldsymbol{x}$), according to the scenario of a nonzero-variate true state (equation (15), solid curve), and the scenario of a zero-variate true state (equation (17b), dashed curve), as a function of SNR. The configurations are detailed in Table 4 and section 4. Clearly the latter scenario (dashed) has a better precision (smaller magnitude) than the former (solid) under the same configuration, i.e., 0.3–1 ppm vs 2.5–3.5 ppm at SNR = 400.

Statistically speaking, the scenario for a zero-variate true state is a special/extreme case of the one discussed in sections 2-3, by demanding a zero covariance $\boldsymbol{S_c}$. Therefore, forcing $\boldsymbol{S_c} = 0$ in (13) yields the distribution of the retrieval quality for a zero-variate CO_2 state vector:

$$(\hat{\boldsymbol{x}} - \boldsymbol{x}) \sim N_n\left(\hat{\boldsymbol{S}}\boldsymbol{S_a}^{-1}(\boldsymbol{x_a} - \boldsymbol{x}), \hat{\boldsymbol{S}}\boldsymbol{K}^T\boldsymbol{S_\varepsilon}^{-1}\boldsymbol{K}\hat{\boldsymbol{S}}\right), \tag{17a}$$

and accordingly for a zero-variate Xco_2 scalar (i.e., using (17a) and (10a)):

$$\left(\boldsymbol{h}^T\hat{\boldsymbol{x}} - \boldsymbol{h}^T\boldsymbol{x}\right) \sim N_1\left(\boldsymbol{h}^T\hat{\boldsymbol{S}}\boldsymbol{S_a}^{-1}(\boldsymbol{x_a} - \boldsymbol{x}),\ \boldsymbol{h}^T\hat{\boldsymbol{S}}\boldsymbol{K}^T\boldsymbol{S_\varepsilon}^{-1}\boldsymbol{K}\hat{\boldsymbol{S}}\boldsymbol{h}\right). \tag{17b}$$

From statistics [e.g., *Anderson*, 2003], equation (17b) reveals that the accuracy and the precision (variance) terms are $\boldsymbol{h}^T\hat{\boldsymbol{S}}\boldsymbol{S_a}^{-1}(\boldsymbol{x_a} - \boldsymbol{x})$ and $\boldsymbol{h}^T\hat{\boldsymbol{S}}\boldsymbol{K}^T\boldsymbol{S_\varepsilon}^{-1}\boldsymbol{K}\hat{\boldsymbol{S}}\boldsymbol{h}$, respectively, for the retrieval quality of a zero-variate Xco_2 true state. Here $\boldsymbol{x}$ is equivalent to its mean $\boldsymbol{x_c}$ since it is zero variate. The physical meaning of (17a) is illustrated schematically in Figure 1b. The scenario of a zero-variate true state (Figure 1b) has the same retrieval accuracy as the nonzero-variate scenario (Figure 1a), but yields a better precision that is purely due to the measurement uncertainty ($\boldsymbol{S_\varepsilon}$). In contrast, the scenario of Figure 1a includes a nonzero covariance $\boldsymbol{S_c}$ (due to a nonzero-variate true state) in (13) that adds an extra uncertainty and hence causes a larger retrieval precision.

As a numerical examination, we perform four experiments that compare the retrieval precision of Xco_2 in these two scenarios [i.e., (17b) vs (15)]. The configurations are summarized in Table 4: the covariance $\boldsymbol{S_c}$ for the nonzero-variate true state [equation (15)) is configured as $(\boldsymbol{S_c})_{ij} = (12\ \text{ppm})^2 \times \exp(-|i-j|/10)$, where the off-diagonal structure is according to section 2.6 of *Rodgers* [2000] and the magnitude (~12 ppm) is according to *Saitoh et al.* [2009]. We apply the similar off-diagonal structure for $\boldsymbol{S_a}$ with various magnitudes (12 ppm, 8 pm, and 4 ppm) in cases 1–3, respectively (detailed in Table 4). In case 4, $\boldsymbol{S_a}$ has a diagonal structure following *Kuang et al.* [2002].

The results are presented in Figure 4: the scenario of a zero-variate true state (dashed curve) always has a better precision (smaller magnitude) than the corresponding scenario of a nonzero-variate true state (solid curve), i.e., 0.3–1 ppm vs 2.5–3.5 ppm at SNR = 400 (the SNR magnitude for OCO-2; Figure 4 cases 1–4). These verify our analytical assessment at the beginning of this section. Note that this contrast above does

Table 4. Configurations of Four Numerical Cases That Contrast the Precision of Xco_2 Retrieval Quality ($\hat{\boldsymbol{x}} - \boldsymbol{x}$) in the Scenario of a Nonzero-Variate True State [Equation (15)] and in the Scenario of a Zero-Variate True State [Equation (17b)], With Results Discussed in Figure 4 and Section 4[a]

	$\boldsymbol{S_a}$
Case 1	$(\boldsymbol{S_a})_{i,j} = (12\ \text{ppm})^2 \times \exp(-\lvert i - j \rvert/10)$
Case 2	$(\boldsymbol{S_a})_{i,j} = (8\ \text{ppm})^2 \times \exp(-\lvert i - j \rvert/10)$
Case 3	$(\boldsymbol{S_a})_{i,j} = (4\ \text{ppm})^2 \times \exp(-\lvert i - j \rvert/10)$
Case 4	$(\boldsymbol{S_a})_{i,i} = (4\ \text{ppm})^2$ diagonal

[a]The covariance $\boldsymbol{S_c}$ for the nonzero-variate true state [equation (15)] is configured as $(\boldsymbol{S_c})_{i,j} = (12\ \text{ppm})^2 \times \exp(-\lvert i - j \rvert/10)$, where the off-diagonal structure is according to section 2.6 of *Rodgers* [2000] and the magnitude (~12 ppm) is according to *Saitoh et al*. [2009]. We apply the similar off-diagonal structure for $\boldsymbol{S_a}$ with various magnitudes (12 ppm to 4 ppm) in cases 1–3, as detailed in this table. In case 4 of this table, $\boldsymbol{S_a}$ has a diagonal structure following *Kuang et al*. [2002]. Here i and j ($i, j = 1, 2, \ldots, 11$) are the indexes for the vertical layers in the model.

not suggest that the former scenario (zero-variate true state) is superior to the latter scenario (nonzero-variate true state): they are designed for *distinct* purposes [i.e., the former aims to measure a snapshot state or abnormally distributed variability, while the latter aims to measure a regularly/Gaussian-distributed variability. The former scenario, however, may have the advantage over the latter in the sense that it is applicable to the abnormally distributed true state and the resulting precision can be exactly quantified even in real-world retrievals (since $\boldsymbol{S_c}$ is zero/known in the former scenario). This above contrast helps to elucidate the statistical feature of the error analysis in these two important scenarios of Xco_2 retrieval (Figure 1a vs 1b).

5. Discussion and Conclusions

In this study, we revisit the methodology of Multivariate Statistics to explore the error analysis for Bayesian-based Xco_2 retrieval from remote sensing.

Our key results are summarized as follows:

1. Rigorous error analysis for OET-based retrieval of CO_2 is often difficult to perform due to the subtlety of Multivariate Statistics. To shed light on this issue, we revisited some fundamentals of Multivariate Statistics (section 2) that are essential to characterize the mathematical nature of the associated error analysis (Figure 1). We show that the related statistical methodology is a practical and useful tool in analyzing the retrieval errors (sections 2–4; the Appendix A).
2. We use the statistical methodology to explore a widely used approximate framework for the error analysis of Xco_2 retrieval [equation (16)], in contrast to a more rigorous framework [equation (15); the Appendix A]. The approximate framework ideally requires the a priori state equal to the true state. Due to the nature of the problem considered, realistic numerical simulations may be more appropriate than remote sensing data for our primary experiments (see the end of section 2). We constructed several empirical configurations to numerically demonstrate these differences. Our experiments show that the approximate framework may potentially yield nonnegligible errors for evaluating the accuracy (Figure 2, up to 0.17–0.28 ppm error at SNR = 400) and the precision (Figure 3, up to 1.4–1.7 ppm error at SNR = 400) of Xco_2 retrieval quality. The errors may become smaller or larger in extensively *various* real-world scenarios, but should statistically become smaller if improving the a priori climatology closer to the true state. This may help to account for the potential missing part of accuracy (up to 0.1–0.3 ppm) and precision (up to 1–2 ppm) underestimated by previous studies that have applied the approximate framework. Our results, however, do not alter the fact that the approximate framework is still useful in real-world remote sensing (see the end of section 2). But the rigorous framework can be a useful benchmark for numerical simulations and in situ measurements.
3. We use the statistical methodology to explore the intrinsic difference and connection for the error analysis between two important remote sensing scenarios: the sounding for a nonzero-variate CO_2 state and the sounding for a zero-variate CO_2 state (snapshot state). Our statistical analysis [equation (17a) vs (13)] and our simulated retrieval experiments suggest that the two scenarios essentially yield the same-magnitude accuracy, while the latter scenario yields a better precision than the former (Figure 4).
4. Our statistical analysis can be applied consistently to the single-sounding scenario or the multiple-sounding scenario (the end of section 3). These two scenarios are intrinsically connected, as reflected by applying the fundamental Multivariate Statistics [e.g., using the theorem equation (11b)].

Our results should be treated with the following caution. First, this note should not be regarded as an exhaustive investigation for OET error analysis, which is a deep subject and far beyond the scope of this note. We focus on the measurement error but do not explicitly include the analysis for the smoothing error and interference error [e.g., *Yoshida et al*., 2011], which should in principle be similarly analyzed by the statistical methodology we discussed here. Second, this note performs the analysis based on the first-order distribution of the optimal solution [equation (5)]. Higher-order nonlinear effects may add an extra nonnegligible uncertainty to the error analysis. Third, the real-world CO_2 state may not necessarily follow Gaussian statistics, which is a known difficulty for error analysis [e.g., *Kulawik et al*., 2006] and can cause complication for our analysis in sections 2-3. Fourth, this note focuses on clear-sky scenarios [*Miller et al*., 2007]. For non-clear-sky conditions, aerosols and clouds can induce extra uncertainties to the accuracy/precision analysis of retrievals [e.g., *Bril et al*., 2007, 2009; *Jiang et al*., 2015]. Fifth, our numerical analysis is carried out in certain parameter spaces [*Kuai et al*., 2010]. Other parameter space is worthy the exploration as well.

Our numerical configurations in section 3, although attempted to be as physical as possible, unavoidably still include idealized components due to the difficulty of parameterizing the true state distribution. As an alternative, in situ measurement like TCCON [*Wunch et al*., 2011] in different regions can *closely* provide some local true-state distribution ($\boldsymbol{x_c}$ and $\boldsymbol{S_c}$). Using this true state data ($\boldsymbol{x_c}$ and $\boldsymbol{S_c}$), rigorous error analysis can be performed according to equation (13) and compare with the results using the approximate framework equation (14). This work can be combined with the studies of *Kulawik et al*. [2016]; *Wunch et al*. [2016], and *Lindqvist et al*. [2015] who recently quantify the quality of satellite GHG retrievals by comparing to TCCON measurements. This observation, if combining with OCO-2 or GOSAT CO_2 retrievals, can be useful to further our exploration on the issue discussed in section 3 (approximate vs rigorous framework). This requires large amounts of work but is our next step. As another future project, we should also test the CO_2 *profile* retrieval [e.g., *Kuai et al*., 2012] in contrast to the Xco_2 retrieval discussed in this study: Using the approximate framework may potentially cause a larger error for the error analysis in profile retrieval than that in Xco_2 retrieval, due to the vertical profile variability.

Our revisiting of methodology, based on the strict Multivariate Statistics, is for a more realistic/*correct* analysis for the contribution of the measurement uncertainty to the retrieval error of CO_2 remote sensing. Our analysis is based on an essential, but often forgotten, fact that a priori climatology in reality is never equal to the true state [*Bowman et al*., 2002]. This methodology is also applicable to the analysis of other types of error such as the forward model errors [since $\boldsymbol{\varepsilon}$ and $\boldsymbol{S_\varepsilon}$ in sections 1-2 can include other types of error; see *Bowman et al*., 2006; *Yoshida et al*., 2011]. Other types of uncertainties will certainly add to our examined retrieval error [*Bösch et al*., 2006; *Li et al*., 2016]. This will be the focus of a future study that will make our current error analysis more complete.

Appendix A: Consistency of Our Equation (13) With Previous Rigorous Studies

As an example from the literature, *Bowman et al*. [2002] perform a rigorous error analysis for the remote sensing retrieval of ozone. They give the covariance of the retrieval quality in their equation (16). Here we show that their equation (16) is consistent with our derived retrieval quality covariance $\hat{\boldsymbol{S}}\left(\boldsymbol{S_a^{-1}S_cS_a^{-1}}+\boldsymbol{K^TS_\varepsilon^{-1}K}\right)\hat{\boldsymbol{S}}$ given in our equation (13) [and hence our equation (15)].

Note that *Bowman et al*. [2002] use different notations from those of *Rodgers* [2000] and *Rodgers and Connor* [2003], while our manuscript follows the notations of the latter throughout. In *Bowman et al*. [2002], $\mathbf{A_{xx}}$ in their equation (16) is the averaging kernel given in their equation (8), which can also be expressed by

$$\mathbf{A}_{xx}=\boldsymbol{GK}=\left(\boldsymbol{K^TS_\varepsilon^{-1}K}+\boldsymbol{S_a^{-1}}\right)^{-1}\boldsymbol{K^TS_\varepsilon^{-1}K}=\hat{\boldsymbol{S}}\boldsymbol{K^TS_\varepsilon^{-1}K}, \tag{A1}$$

according to equations (2.58), (2.45) and (2.27) of *Rodgers* [2000]. Here $\hat{\boldsymbol{S}}$ is given by our equation (6). It is straightforward to show

$$\mathbf{I}-\mathbf{A}_{xx}=\mathbf{I}-\hat{\boldsymbol{S}}\boldsymbol{K^TS_\varepsilon^{-1}K}=\hat{\boldsymbol{S}}\left(\hat{\boldsymbol{S}}^{-1}-\boldsymbol{K^TS_\varepsilon^{-1}K}\right)=\hat{\boldsymbol{S}}\boldsymbol{S_a^{-1}}. \tag{A2}$$

Further, $\mathbf{S_x}$ in equation (16) of *Bowman et al*. [2002] is the covariance of the true state vector $\boldsymbol{x}$ given in their equation (12), which is denoted as $\mathbf{S_c}$ in our manuscript. Therefore, according to (A2), $(\mathbf{I}-\mathbf{A_{xx}})\mathbf{S_x}(\mathbf{I}-\mathbf{A_{xx}})^{\mathsf{T}}$ in equation (16) of *Bowman et al*. [2002] can be expressed by

$$(\mathbf{I}-\mathbf{A}_{xx})\mathbf{S}_x(\mathbf{I}-\mathbf{A}_{xx})^T = \hat{\boldsymbol{S}}\boldsymbol{S}_a^{-1}\,\boldsymbol{S}_c\left(\hat{\boldsymbol{S}}\boldsymbol{S}_a^{-1}\right)^{\boldsymbol{T}} = \hat{\boldsymbol{S}}\,\boldsymbol{S}_a^{-1}\,\boldsymbol{S}_c\boldsymbol{S}_a^{-1}\,\hat{\boldsymbol{S}}. \tag{A3}$$

There is a factor $\mathbf{MG_z}$ in their equation (16). Contrasting their equation (8) with our (A1) above, $\mathbf{MG_z}$ can be expressed by

$$\mathbf{MG_z} = \hat{\boldsymbol{S}}\boldsymbol{K}^{\boldsymbol{T}}\boldsymbol{S}_{\varepsilon}^{-1}. \tag{A4}$$

Next, $\mathbf{S_n}$ in their equation (16) is the error covariance [see their equation (1) and the definition of $\mathbf{S_n}$ there), which is denoted as $\boldsymbol{S}_{\varepsilon}$ in our manuscript. Therefore, from (A4), $\mathbf{MG_z}\boldsymbol{S_n}\ \mathbf{G_z^{\mathsf{T}}}\ \mathbf{M^{\mathsf{T}}}$ in their equation (16) can be expressed as follows:

$$\mathbf{MG_z}\mathbf{S}_n\mathbf{G_z^{\mathsf{T}}}\mathbf{M^{\mathsf{T}}} = \hat{\boldsymbol{S}}\boldsymbol{K}^{\boldsymbol{T}}\boldsymbol{S}_{\varepsilon}^{-1}\boldsymbol{S}_{\varepsilon}\left(\hat{\boldsymbol{S}}\boldsymbol{K}^{\boldsymbol{T}}\boldsymbol{S}_{\varepsilon}^{-1}\right)^{\boldsymbol{T}} = \hat{\boldsymbol{S}}\boldsymbol{K}^{\boldsymbol{T}}\boldsymbol{S}_{\varepsilon}^{-1}\boldsymbol{S}_{\varepsilon}\,\boldsymbol{S}_{\varepsilon}^{-1}\boldsymbol{K}\hat{\boldsymbol{S}} = \hat{\boldsymbol{S}}\boldsymbol{K}^{\boldsymbol{T}}\boldsymbol{S}_{\varepsilon}^{-1}\boldsymbol{K}\hat{\boldsymbol{S}} \tag{A5}$$

Finally, we combine equations (A3) and (A5) and hence obtain the alternative expression for equation (16) of *Bowman et al*. [2002]:

$$\begin{aligned}(\mathbf{I}-\mathbf{A}_{xx})\mathbf{S}_x(\mathbf{I}-\mathbf{A}_{xx})^T + \mathbf{MG_z}\mathbf{S}_n\mathbf{G_z^{\mathsf{T}}}\mathbf{M^{\mathsf{T}}} &= \hat{\boldsymbol{S}}\boldsymbol{S}_a^{-1}\,\mathbf{S}_c\boldsymbol{S}_a^{-1}\hat{\boldsymbol{S}} + \hat{\boldsymbol{S}}\boldsymbol{K}^{\boldsymbol{T}}\boldsymbol{S}_{\varepsilon}^{-1}\boldsymbol{K}\hat{\boldsymbol{S}}\\ &= \hat{\boldsymbol{S}}\left(\boldsymbol{S}_a^{-1}\,\mathbf{S}_c\boldsymbol{S}_a^{-1} + \boldsymbol{K}^{\boldsymbol{T}}\boldsymbol{S}_{\varepsilon}^{-1}\boldsymbol{K}\right)\hat{\boldsymbol{S}}\end{aligned} \tag{A6}$$

This is exactly the same as the covariance of the retrieval quality given in our equation (13). Therefore, our equation (13) is consistent with *Bowman et al*. [2002] regarding the rigorous framework of error analysis.

Acknowledgments
We gratefully acknowledge the helpful comments/suggestions from three anonymous reviewers and the Editor. We thank Paul O. Wennberg, John Worden, Vijay Natraj, Michael Line, King-Fai Li for useful comments/discussions, and Le Kuai for providing the model used in this study. This research is supported in part by the Orbiting Carbon Observatory (OCO-2) project, a NASA Earth System Science Pathfinder (ESSP) mission, and JPL P765982 grant to the California Institute of Technology.

References

Anderson, T. W. (2003), *An Introduction to Multivariate Statistical Analysis*, 721 pp., John Wiley, New York.
Lindqvist, H., et al. (2015), Does GOSAT capture the true seasonal cycle of carbon dioxide?, *Atmos. Chem. Phys.*, *15*, 13,023–13,040.
Basilevsky, A. (1994), *Statistical Factor Analysis and Related Methods: Theory and Applications*, 737 pp., John Wiley, New York.
Boesch, H., D. Baker, B. Connor, D. Crisp, and C. Miller (2011), Global characterization of CO2 column retrievals from shortwave-infrared satellite observations of the Orbiting Carbon Observatory-2 mission, *Remote Sens.*, *3*(2), 270–304.
Bösch, H., et al. (2006), Space-based near-infrared CO2 measurements: Testing the Orbiting Carbon Observatory retrieval algorithm and validation concept using SCIAMACHY observations over Park Falls, Wisconsin, *J. Geophys. Res.*, *111*, 23302, doi:10.1029/2006JD007080.
Bovensmann, H., M. Buchwitz, J. P. Burrows, M. Reuter, T. Krings, K. Gerilowski, O. Schneising, J. Heymann, A. Tretner, and J. Erzinger (2010), A remote sensing technique for global monitoring of power plant CO_2 emissions from space and related applications, *Atmos. Meas. Tech.*, *3*(4), 781–811.
Bowman, K. W., T. Steck, H. M. Worden, J. Worden, S. Clough, and C. Rodgers (2002), Capturing time and vertical variability of tropospheric ozone: A study using TES nadir retrievals, *J. Geophys. Res.*, *107*(D23), 4723, doi:10.1029/2002JD002150.
Bowman, K. W., et al. (2006), Tropospheric Emission Spectrometer: Retrieval method and error analysis, *IEEE Trans. Geosci. Remote Sens.*, *44*(5), 1297–1307.
Bril, A., S. Oshchepkov, T. Yokota, and G. Inoue (2007), Parameterization of aerosol and cirrus cloud effects on reflected sunlight spectra measured from space: Application of the equivalence theorem, *Appl. Opt.*, *46*(13), 2460–2470.
Bril, A., S. Oshchepkov, and T. Yokota (2009), Retrieval of atmospheric methane from high spectral resolution satellite measurements: A correction for cirrus cloud effects, *Appl. Opt.*, *48*(11), 2139–2148.
Buchwitz, M., et al. (2012), *The GHG-CCI project of ESA's Climate Change Initiative: Overview and Status*, *proc. ESA ATMOS 2012 conf.*, vol. 708, ESA Spec. Publ. SP, Bruges, Belgium.
Connor, B., et al. (2016), Quantification of uncertainties in OCO-2 measurements of XCO 2: Simulations and linear error analysis, *Atmos. Meas. Tech.*, *9*, 5227–5238.
Connor, B. J., H. Boesch, G. Toon, B. Sen, C. Miller, and D. Crisp (2008), Orbiting Carbon Observatory: Inverse method and prospective error analysis, *J. Geophys. Res.*, *113*, D05305, doi:10.1029/2006JD008336.
Cressie, N., R. Wang, M. Smyth, and C. E. Miller (2016), Statistical bias and variance for the reg ularized inverse problem: Application to space-based atmospheric CO2 retrievals, *J. Geophys. Res. Atmos.*, *121*, 5526–5537, doi:10.1002/2015JD024353.
Crisp, D., et al. (2016), The OnOrbit Performance of the Orbiting Carbon Observatory2 (OCO2) Instrument and its Radiometrically Calibrated Products, *Atmos. Meas. Tech.*, *10*, 59–81.
Eguchi, N., R. Saito, T. Saeki, Y. Nakatsuka, D. Belikov, and S. Maksyutov (2010), A priori covariance estimation for CO_2 and CH_4 retrievals, *J. Geophys. Res.*, *115*, D10215, doi:10.1029/2009JD013269.
Frankenberg, C., et al. (2015), The Orbiting Carbon Observatory (OCO-2): Spectrometer performance evaluation using pre-launch direct sun measurements, *Atmos. Meas. Tech.*, *8*(1), 301–313.
Fu, D., T. J. Pongetti, J.-F. L. Blavier, T. J. Crawford, K. S. Manatt, G. C. Toon, C. Wong, and S. P. Sander (2014), Near-infrared remote sensing of Los Angeles trace gas distributions from a mountaintop site, *Atmos. Meas. Tech.*, *7*(3), 7713–7729.
Hammerling, D. M., A. M. Michalak, and S. R. Kawa (2012), Mapping of CO2 at high spatiotemporal resolution using satellite observations: Global distributions from OCO-2, *J. Geophys. Res.*, *117*, D06306, doi:10.1029/2011JD017015.
Härdle, W., and L. Simar (2007), *Applied Multivariate Statistical Analysis*, vol. 22007, Springer, Berlin.
Jiang, J. H., et al. (2015), Evaluating the diurnal cycle of upper tropospheric ice clouds in climate models using SMILES observations, *J. Atmos. Sci.*, *72*, 1022–1044.

Jiang, X., M. T. Chahine, E. T. Olsen, L. Chen, Y. L. Yung (2010), Interannual variability of midtropospheric CO_2 from Atmospheric Infrared Sounder, *Geophys. Res. Lett.*, *37*, L13801, doi:10.1029/2010GL042823.

Jiang, X., J. Wang, E. T. Olsen, T. Pagano, L. L. Chen, and Y. L. Yung (2013), Influence of stratospheric sudden warming on AIRS mid-tropospheric CO_2, *J. Atmos. Sci.*, *70*, 2566–2573.

Jiang, X., D. Crisp, E. T. Olsen, S. S. Kulawik, C. E. Miller, T. S. Pagano, M. Liang, and Y. L. Yung (2016), CO_2 annual and semiannual cycles from multiple satellite retrievals and models, *Earth Space Sci.*, *3*, 78–87.

Keppel-Aleks, G., P. O. Wennberg, and T. Schneider (2011), Sources of variations in total column carbon dioxide, *Atmos. Chem. Phys.*, *11*, 3581–3593.

Kuai, L., V. Natraj, R.-L. Shia, C. Miller, and Y. L. Yung (2010), Channel selection using information content analysis: A case study of CO_2 retrieval from near infrared measurements, *J. Quant. Spectros. Radiat. Transfer*, *111*(9), 1296–1304.

Kuai, L., D. Wunch, R.-L. Shia, B. Connor, C. Miller, and Y. Yung (2012), Vertically constrained CO2 retrievals from TCCON measurements, *J. Quant. Spectros. Radiat. Transfer*, *113*(14), 1753–1761.

Kuang, Z., J. Margolis, G. Toon, D. Crisp, and Y. Yung (2002), Spaceborne measurements of atmospheric CO2 by high-resolution NIR spectrometry of reflected sunlight: An introductory study, *Geophys. Res. Lett.*, *29*(15), 1716, doi:10.1029/2001GL014298.

Kulawik, S., G. Osterman, D. B. A. Jones, and K. W. Bowman (2006), Calculation of altitude-dependent Tikhonov constraints for TES nadir retrievals, *IEEE Trans. Geosci. Remote Sens.*, *44*, 1334–1342.

Kulawik, S., et al. (2016), Consistent evaluation of ACOS-GOSAT, BESD-SCIAMACHY, CarbonTracker, and MACC through comparisons to TCCON, *Atmos. Meas. Tech.*, *9*, 683–709.

Li, Y., et al. (2016), CO2 retrieval model and analysis in short-wave infrared spectrum, *Optik-Int. J. Light Electron Optics*, *127*(10), 4422–4425.

Miller, C., et al. (2007), Precision requirements for space-based XCO_2 data, *J. Geophys. Res.*, *112*, D10314, doi:10.1029/2006JD007659.

O'Brien, D., I. Polonsky, and C. W. O'Dell (2009), Orbiting carbon observatory algorithm theoretical basis document: The OCO simulator, *Tech. Rep.*, p. 148, Coop. Inst. for Res. in the Atmos., Fort Collins, Colo.

O'Dell, C. W., et al. (2012), The ACOS CO2 retrieval algorithm—Part 1: Description and validation against synthetic observations, *Atmos. Meas. Tech.*, *5*, 99–121.

Reuter, M., M. Buchwitz, O. Schneising, J. Heymann, H. Bovensmann, and J. P. Burrows (2010), A method for improved SCIAMACHY CO_2 retrieval in the presence of optically thin clouds, *Atmos. Meas. Tech.*, *3*, 209–232.

Reuter, M., et al. (2011), Retrieval of atmospheric CO_2 with enhanced accuracy and precision from SCIAMACHY: Validation with FTS measurements and comparison with model results, *J. Geophys. Res.*, *116*, D04301, doi:10.1029/2010JD015047.

Reuter, M., M. Buchwitz, O. Schneising, J. Heymann, S. Guerlet, A. J. Cogan, H. Bovensmann, and J. P. Burrows (2012), A simple empirical model estimating atmospheric CO_2 background concentrations, *Atmos. Meas. Tech.*, *5*, 1349–1357.

Rodgers, C. D. (1976), Retrieval of atmospheric temperature and composition from remote measurements of thermal radiation, *Rev. Geophys.*, *14*(4), 609–624, doi:10.1029/RG014i004p00609.

Rodgers, C. D. (2000), *Inverse Methods for Atmospheric Sounding: Theory and Practice*, pp. 238, World Sci., Hackensack, N. J.

Rodgers, C. D., and B. J. Connor (2003), Intercomparison of remote sounding instruments, *J. Geophys. Res.*, *108*(D3), 4116, doi:10.1029/2002JD002299.

Saitoh, N., R. Imasu, Y. Ota, and Y. Niwa (2009), CO2 retrieval algorithm for the thermal infrared spectra of the Greenhouse Gases Observing Satellite: Potential of retrieving CO_2 vertical profile from high-resolution FTS sensor, *J. Geophys. Res.*, *114*, D17305, doi:10.1029/2008JD011500.

Su, Z., X. Xi, V. Natraj, K.-F. Li, R.-L. Shia, C. E. Miller, and Y. L. Yung (2015), Information-rich spectral channels for simulated retrievals of partial column-averaged methane, *Earth Space Sci.*, *3*, 2–14.

Tabachnick, B. G., and L. S. Fidell (2013), *Using Multivariate Statistics*, Pearson, Boston.

Taylor, J. R. (1999), *An Introduction to Error Analysis: The Study of Uncertainties in Physical Measurements*, Univ. Science Books, Mill Valley, Calif.

Tong, Y. (1990), *The Multivariate Normal Distribution*, Springer, New York.

Worden, J., S. S. Kulawik, M. W. Shephard, S. A. Clough, H. Worden, K. Bowman, and A. Goldman (2004), Predicted errors of tropospheric emission spectrometer nadir retrievals from spectral window selection, *J. Geophys. Res.*, *109*, D09308, doi:10.1029/2004JD004522.

Wunch, D., G. C. Toon, J.-F. L. Blavier, R. A. Washenfelder, J. Notholt, B. J. Connor, D. W. Griffith, V. Sherlock, and P. O. Wennberg (2011), The total carbon column observing network, *Philos. Trans. R. Soc. London, Ser. A*, *369*(1943), 2087–2112.

Wunch, D., et al. (2016), Comparisons of the Orbiting Carbon Observatory-2 (OCO-2) XCO2 measurements with TCCON, *Atmos. Meas. Tech. Discuss.*, doi:10.5194/amt-2016-227.

Yoshida, Y., Y. Ota, N. Eguchi, N. Kikuchi, K. Nobuta, H. Tran, I. Morino, and T. Yokota (2011), Retrieval algorithm for CO_2 and CH_4 column abundances from short-wavelength infrared spectral observations by the Greenhouse gases observing satellite, *Atmos. Meas. Tech.*, *4*(4), 717–734.

Zeng, Z., et al. (2012), A spatio-temporal interpolation approach for the FTS SWIR product of XCO2 data from GOSAT, in *Proc. IEEE Int. Geosci. Remote Sens. Symp*, pp. 852–855, IGARSS, Munich, Germany.

Zeng, Z., L. Lei, S. Hou, F. Ru, X. Guan, and B. Zhang (2014), A Regional Gap-Filling Method Based on Spatiotemporal Variogram Model of CO2 Columns, *IEEE Trans. Geosci. Remote Sens.*, *52*, 3594–3603.